Hindawi Publishing Corporation
International Journal of Photoenergy
Volume 2012, Article ID 261045, 10 pages
doi:10.1155/2012/261045

Research Article

Performance of Ag-TiO_2 Photocatalysts towards the Photocatalytic Disinfection of Water under Interior-Lighting and Solar-Simulated Light Irradiations

Camilo A. Castro, Adriana Jurado, Diana Sissa, and Sonia A. Giraldo

Centro de Investigaciones en Catálisis (CICAT), Universidad Industrial de Santander, Cra. 27 Calle 9, A.A. 678 Bucaramanga, Colombia

Correspondence should be addressed to Sonia A. Giraldo, sgiraldo@uis.edu.co

Received 14 July 2011; Accepted 19 August 2011

Academic Editor: Jiaguo Yu

This paper reports the characterization and photoactivity of Ag-TiO_2 materials using different amounts of silver during the hydrothermal synthesis. Photocatalysts were characterized by means of TEM, XPS, XRD, DRS, and N_2 sorption isotherms to determine the textural properties. The photocatalyst's configuration was observed to be as anatase-brookite mixed phase particles with Ag partially oxidized aggregates on the TiO_2 surface, which increased visible light absorption of the material. Moreover, photoproduction of singlet oxygen was followed by EPR analysis under visible light irradiations following the formation of TEMPOL. Such photoproduction was totally decreased by using the singlet oxygen scavenger DABCO. Photocatalysts were tested towards the photocatalytic disinfection of water suing a solar light simulator and an interior-light irradiation setup. Results evidenced an increase in the photooxidative effect of TiO_2, while dark processes evidenced that part of the inactivation process is due to the Ag-TiO_2 surface bactericidal effect and possible lixiviated Ag^+.

1. Introduction

The design of TiO_2-based photoactive materials has been a major research topic during the last two decades [1–3]. TiO_2, as a semiconductor, is activated under UV irradiation promoting charges that lead to the formation of reactive oxygen species when they interact with H_2O and O_2 from the reaction media. Nowadays, recombination of the photogenerated charges [4, 5] and visible (vis) light response [4] are two drawbacks still to surpass in order to achieve efficient photocatalysts to be used under solar light or interior-lighting irradiations.

Water disinfection using TiO_2 had attracted research interest since the oxidative attack of photoproduced ROS may cause total inactivation of bacteria [6, 7] without generating harmful byproducts [8]. In order to increase its photooxidative effect, towards bacteria inactivation, TiO_2 has been modified with Ag, which increases vis light absorption [9–11] and has been proposed to decrease recombination [12], on TiO_2 thin films [12] and powdered materials [13]. New insights have proposed electronic transitions arising from vis-excited Ag aggregates to the TiO_2 conduction band promoting its photobactericidal effect [14], as it has been observed on plasmonic photocatalysis [10]. Furthermore, Ag-containing antimicrobial devices are designed due to the well-known Ag bacteriostatic activity [15].

Ag-modified TiO_2 photocatalysts have been synthesized using the hydrothermal method since this is a relatively simple route to load TiO_2 nanoparticles with Ag [16, 17], with a wide range of optimum silver content from 0.1 to 6.5% wt correspondent to the major increase in photoactivity [11, 18, 19]. Ag has been proposed to be as aggregates located in crystals borders of TiO_2 particles [20, 21]. Since Ag^+ and Ti^{4+} ionic radii are 1.16 [22] and 0.64 Å [23], respectively, it is not expected that Ag may be embedded into the TiO_2 structure.

The aim of this work is to present the performance of Ag-TiO_2 photocatalyst, obtained using the hydrothermal synthesis route, under different light irradiations setups such as

solar-simulated and interior-lighting lamps with different irradiation powers, towards the photocatalytic inactivation of *E. coli* in water. Moreover, materials were characterized using TEM, XPS, DRS, and N_2 adsorption-desorption isotherms in order to elucidate properties affecting the photoactivity. Results show an effective modification of TiO_2 with enhanced visible light absorption capacity as well as photoactivity.

2. Experimental

2.1. Photocatalyst Synthesis. Photocatalysts were hydrothermal synthesized as follows: 3.8 mL of titanium butoxide (99.9%, Fluka) was added dropwise to 19 mL of isopropanol (Suprasolv. grade reagent, Merck). Then, an adequate amount of $AgNO_3$ (Extra pure, Merck) was diluted in 2 mL of water (pH = 1.5) adjusted with HNO_3 (65%, Merck). Ag aqueous solution was added dropwise to the isopropoxide-isopropanol solution with an appropriate concentration to obtain Ag nominal weight percentages (% wt), of 0.5, 2, 4, and 8. Formed gel was steam-pressure-treated in autoclave during 3 h at 120°C and ~144 KPa. TiO_2 was obtained as described without addition of $AgNO_3$. The obtained wet crystals were grounded in mortar, dried in oven at 60°C for 12 h, and kept in dark to avoid surface oxidation. Samples were labeled as Ag(x)-TiO_2, x = Ag % wt.

2.2. Photocatalyst Characterization. Fresh Ag(x)-TiO_2 and TiO_2 samples were XPS-analyzed. To follow Ag states after a typical photocatalytic test a Ag(2)TiO_2 suspension, without *E. coli*, was submitted 2 h to solar-simulated light irradiation, filtered and dried in oven at 60°C, and then XPS-analyzed. Analyses were carried out using an AXIS-NOVA photoelectron-spectrometer (Kratos-analytical, Manchester, UK) equipped with a monochromatic AlKα ($h\nu$ = 1486.6 eV) anode. Electrostatic-charge effect was overcompensated by means of the low-energy electron source working in combination with a magnetic immersion lens. C1s line at 284.8 eV was used as calibration reference. Spectra were decomposed using the CasaXPS program (Casa Software Ltd., UK) with a Gaussian/Lorentzian (70/30) product function after subtraction of a Shirley baseline. Assignment of Ag and Ti states was restricted using peak distances of 6 eV and 5.3 eV for Ag [12] and Ti [24], respectively.

X-ray diffraction (XRD) patterns were collected using a DMax-IIIB Rigaku system operated at room temperature, 40 kV and 80 mA with monochromatic Cu-Kα radiation. The average crystallite size (d_{XRD}) was calculated using the Scherrer equation applied to anatase peaks at $2\theta = 25.2°$ on samples' diffractograms. Al_2O_3 corundum oxide was used to quantify crystalline phases for bare TiO_2 and the highest Ag loading in order to identify possible changes in phase composition and crystallinity due to Ag loading for modification.

Diffusive reflectance spectroscopy (DRS) was done using a UV-2401PC Shimadzu spectrophotometer with an ISR240A integrating sphere accessory. $BaSO_4$ was used as reference.

Transmission Electron Microscopy (TEM) analysis were performed in a Phillips HRTEM CM 300 (field emission gun, 120 kV) microscope.

Textural analyses of the photocatalysts were performed through N_2 adsorption-desorption isotherms obtained at 77 K in a Nova1200 equipment of Quantachrome. Before the analysis 0.15–0.2 g samples were degasified during 12 h at 373 K under 10^{-5} mmHg vacuum. Specific surface area (S_{BET}) and average pore diameter (d_p) were obtained by means of BET and BJH methods, respectively.

Reactive scavenging of ROS by electron paramagnetic resonance spectroscopy (EPR) was done using 2 mL of 0.3 g/L Ag(2)-TiO_2 suspension and 5×10^{-2} mol/L of 2,2,6,6-tetramethyl-4-piperidinol (TMP-OH, 99%, Fluka), with spectral parameters: $\mathbf{D}_H$ = 1.58 G, $\mathbf{a}_N$ = 16.9 G, and $\mathbf{g}$ = 2.0066, and was prepared in ultrapure H_2O, as well as, in D_2O (99.9% atomic purity, Aldrich). 1,4-diazabicyclo [2,2,2] octane (DABCO, 99%, Fluka) was used as a singlet oxygen quencher [25]. Suspensions were kept in test tubes and ultrasound treated in a water bath with a frequency of 40 kHz for 1 min prior to illumination. 1 mL aliquot of the suspension was transferred into a 5 mL Pyrex beaker and exposed to illumination under constant magnetic stirring with a white light halogen spot source of 150 W from OSRAM reference Gx5.3 (93638) emitting vis. ~7 μL aliquots of the illuminated suspensions were transferred into glass capillary tubes 0.7 mm ID and 0.87 mm OD, from VitroCom, NJ, USA. Tubes were sealed on both ends with Cha-Seal tube-sealing compound (Medex International, Inc., USA). To maximize sample volume in the active zone of the ESR cavity, assemblies of seven packed capillaries were positioned in a wider quartz capillary (standard ESR tube, 2.9 mm ID and 4 mm OD, Wilmad-LabGlass, Vineland, NJ, USA). Such setup resulted in ~65 μL sample volume in the active zone of the ESR cavity, thus markedly improving sensitivity of measurements [26].

Experiments were performed using an ESR300 spectrometer (Bruker-BioSpin-GmbH) at room temperature, equipped with standard-rectangular mode TE_{102} cavity. Routinely, for each experimental point five scan field-swept spectra were recorded with instrumental parameters: microwave frequency: 9.38 GHz, microwave power: 2.0 mW, sweep width: 120 G, modulation frequency: 100 kHz, modulation amplitude: 0.5 G, receiver gain: 4×10^{-4}, time constant: 20.48 ms, conversion time: 40.96 ms, and time per single scan: 41.9 s. Acquired EPR traces correspond to the second derivative of the sample's paramagnetic absorption.

2.3. Photocatalytic Activity. Photobactericidal activity was measured by sampling *E.coli* strain ATCC 11229 from Pyrex photoreactors with a 50 mL of a 0.1 g/L TiO_2 suspension. Before experiments, bacteria were inoculated into Luria Bertani growth media (1% wt, tryptone from Oxoid, 0.5% wt yeast extract from Oxoid, and 1% wt NaCl from Merck) and grown during 8 h at 37°C. During the stationary growth phase, bacteria were harvested by centrifugation at 5000 rpm for 10 min at 4°C. The obtained bacterial pellet was washed three times with saline solution (8 g/L NaCl, 0.8 g/L KCl in Milli-Q water, pH = 7 by addition of HCl or NaOH). A suitable cell concentration (10^7 colony forming units (CFU) per mL) was inoculated to reactors suspensions. Then, photocatalyst was added to each reactor. Suspensions were illuminated during 2 h, and samples (1 mL) were taken at

different time intervals. Serial dilutions were performed in saline solution and 10 μL samples were inoculated 4 times in plate count agar (PCA, Merck). The number of colonies was counted after 24 h of incubation at 37°C.

E. coli + TiO_2 suspensions were kept under magnetic stirring and illuminated under two different lamp setups: (1) 67 lx of white light illumination, with 9.8 W/m^2 of irradiation, using a set of 5 natural sunshine light Phillips lamps (20 W), respectively, with emission between 360 and 700 nm or (2) 250 or 400 W/m^2 of solar-simulated light irradiation using a suntest system model CPS+ from ATLAS, with temperature and irradiation power control, and a Xenon lamp emitting light with wavelengths of 300 y 800 nm, and 5% of the irradiation corresponds to UV-A. The radiant flux was monitored with a Kipp & Zonen (CM3) power meter (Omni instruments Ltd., Dundee, UK) and a Hagner EC1 digital luxmeter.

Bacteria concentration was also followed in dark suspended and stirred Ag-TiO_2 and TiO_2 suspensions to analyze possible induced dead by toxicity of the materials. Moreover, to analyze possible lixiviation of Ag^+ ions an Ag(2)TiO_2 suspension was stirred under darkness for 10 h and then filtered. Since *E. coli* is inactivated by Ag^+ ions in solution it is possible then to determine if lixiviated Ag may decrease bacteria concentration [27]. Thus, *E. coli* was added to the filtered solution and bacteria concentration was determined by intervals of 2 h under darkness.

An additional determination of the *E. coli* concentration was made in order to analyze the time needed for effective disinfection. In this case a sample of each reactor with Ag-TiO_2 photocatalysts was taken after 1 h of irradiation and kept under darkness for 24 h. After this period the samples were submitted to plating and incubation as already described, and finally, colonies were counted on agar plates. The effective irradiation time (EDT) for inactivation was assigned to the sample with zero bacteria counting after 24 h under darkness and was labeled as EDT_{24}.

3. Results and Discussion

3.1. Photocatalysts Features. The optical response of the samples has been followed by means of the spectral response on DRS analyses. Figure 1 shows the DRS spectra of the TiO_2- and Ag-modified TiO_2 samples. TiO_2 spectrum consists of a wide absorption band below ~370 nm ascribed to electron transitions from the valence band (VB), to the conduction band (CB) [28]. Moreover, an interesting light response was found for Ag-loaded samples. Increase in Ag concentration induces a shift in light absorption to the vis range for wavelengths up to 800 nm. DRS spectrum of the 0.5% Ag-loaded TiO_2 sample did not show a significant increase in visible absorption capacity of the material, thus results are not presented. In addition, the 8% Ag-loaded sample shows a shoulder-like peak at ~460 nm which has been proposed for Ag^0 nanoparticles inducing vis light absorption [29]. Atoms, ions, and clusters of silver show characteristic absorption peaks with irradiation wavelengths from 190 nm 500 nm in DRS spectra. Bands at 190–230 nm ascribed to $4d^{10}$–$4d^9 5s^1$

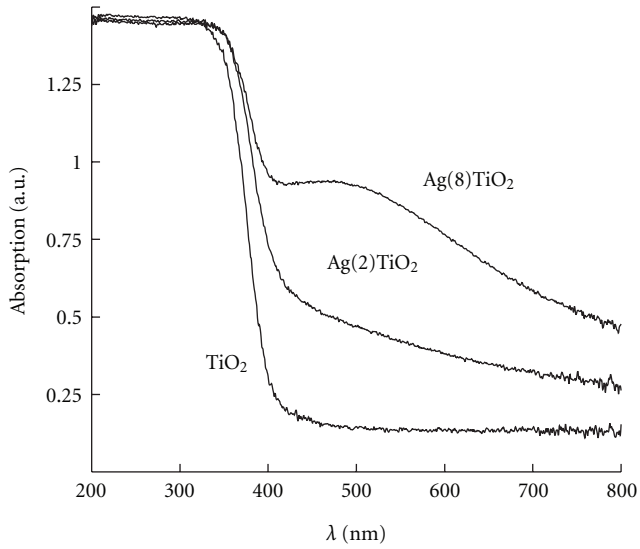

Figure 1: DRS spectra of the TiO_2 and Ag-TiO_2 samples.

transitions in Ag^+, while those at 250–330 nm attributed to $4d^{10}5s^1$–$4d^9 5s^1 5p^1$, $4d^{10}5s^1$–$4d^9 5s^1 6p^1$, or $5s^1$–p^1 transitions in Ag^0 [30], are overlapped by VB-to-CB transitions on TiO_2 as previously observed. In addition, $Ag_n^{\delta+}$ clusters (where n is in the range 2–13, and $\delta = n - 1$) with $n > 3$ present three absorption bands at 360, 460, and 500 nm [31]. Bands at 350–380 nm are attributed to Ag clusters of ~1 nm size, while clusters of 10 nm size and crystallites absorb at 400–500 nm [30, 31].

Such shoulder-like peak has been observed for Ag nanoparticles inducing collective oscillations of the conduction band electrons with the incident light [32, 33]. This effect has also been observed for Au and Pt nanoparticles [34]. This electromagnetic resonance is known as a surface plasmon resonance effect which in this case may induce photoactivity of TiO_2 under vis irradiation [35] as it will be discussed.

In contrast, a slight decrease in the slope of the absorption threshold is observed due to Ag loading of TiO_2. Such decrease is related to a decrease in the energy bandgap. Probably, the increase in N residues coming from the Ag salt precursor, $AgNO_3$, may lead to new intrabandgap states promoting electronic transitions of lower energy requirements between N and the TiO_2 conduction band, thus leading to a decrease in the energy gap [36]. However, as we have stated, in a previous work, NO_3^- residues in Fe-TiO_2 samples, obtained by the hydrothermal route, do not promote photoactivity under vis light [4]. Therefore, DRS spectra observed in Figure 1 suggest that increased absorption due to Ag presence, with a peak at ~460 nm, is possibly due to the localized surface plasmon resonance of Ag nanoparticles [37, 38].

Figure 2 shows the emission spectra of the chosen light setups. The Xenon and interior-lighting lamps have similar distribution spectra between 300 and 800 nm. Both lamps have low emissions under 400 nm in comparison to the emissions in the vis range (400–800 nm). This is supposed to activate TiO_2 alone since its absorption threshold lies at 400 nm

as observed in Figure 1. However, the major part of both emission spectra suggests that vis irradiation predominates over UV irradiation thus giving the chance to activate surface Ag aggregates.

Figure 3 shows the X-ray diffractograms of samples. Anatase (A) is identified as the primary crystalline phase in both samples with peaks at 2θ of 25.2°, 37.9°, 48.2°, 55.0°, and 62.6°. In addition, a slight peak at 30.7° assigned to brookite (B) is observed for all samples. Al_2O_3 corundum (C) peaks are observed for TiO_2 and Ag(8)TiO_2 samples' diffractogram since this oxide was used in the quantification of the phase composition of these two samples, while Ag-related phases were not identified in any of the samples due to low concentrations. Ag loading did not cause significant changes in crystallinity since, as previously described, Ag^+ ion radii is too large to replace Ti^{4+} ions in the TiO_2 matrix. Furthermore, on quantitative XRD analysis it was determined that TiO_2 sample is constituted of anatase, brookite, and amorphous in percentages of 38.4, 12.2, and 49.2%, respectively, while those for Ag(8)TiO_2 are 39, 9.2, and 51.8%, respectively. As a consequence, since Ag does not change phase structure aggregates may be formed on crystal borders and on the surface of the photocatalyst, thus promoting vis light absorption as discussed in Figure 1.

Table 1 shows the calculated average crystallite size and some textural properties of the samples. A slight decrease in crystallite size was observed due to Ag loading probably due to obstruction to anatase crystallite growth by Ag aggregates located in crystal borders. Fe^{3+} modifications on TiO_2, using the same hydrothermal synthesis, promoted changes on the crystalline structure due to its similarity in sizes with Ti^{4+} ions, thus replacing Ti atoms and decreasing crystallite size [4]. Therefore, it is possible to suggest that during the synthesis Ag aggregates are deposited on the surface or grain boundaries.

TEM micrographs of the TiO_2 and Ag(2)TiO_2 samples are shown in Figure 4. As observed, the TiO_2 sample is constituted of irregular particles with approximate sizes of 8–10 nm. The difference between d_{XRD} and the observed particle size in TEM analysis is due to agglomeration of crystallites. In addition, the Ag(2)TiO_2 micrograph shows a similar size distribution to that of bare TiO_2 as it was previously suggested in XRD analyses. Moreover, previously suggested Ag nanoparticles were not observed during the analysis probably due to low resolution of equipment.

Textural properties evidence mesoporous materials with high area. Ag loading caused a significant decrease in S_{BET} probably due to deposition of Ag aggregates on the TiO_2 surface thus leading to pore obstruction [39]. Figure 5 shows type IV isotherms for TiO_2 and Ag(2)TiO_2 samples. Moreover, the sorption isotherm of the TiO_2 sample demonstrated a hysteresis pattern between types H1 and H2, while that of the Ag(2)TiO_2 sample shows a type H2 hysteresis loop. Type H1 loops are often assigned to agglomerates or compact or spherical particles with uniform size, while type H2 loops are attributed to pore size and shape distributions not well defined [40]. Therefore, it is possible to suggest that Ag modification distorted the distribution of pores of the mesoporous structure of TiO_2 due to location of Ag aggregates on grain boundaries, as previously suggested.

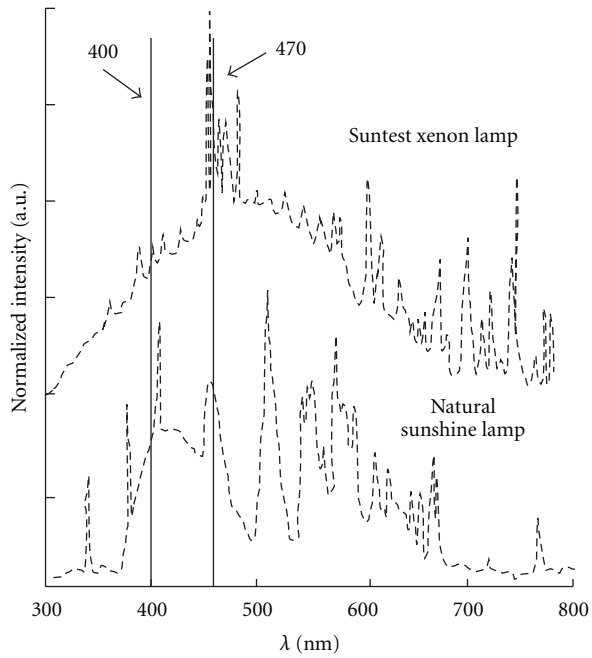

Figure 2: Emission spectra of the Xenon and natural sunshine lamps for interior lighting.

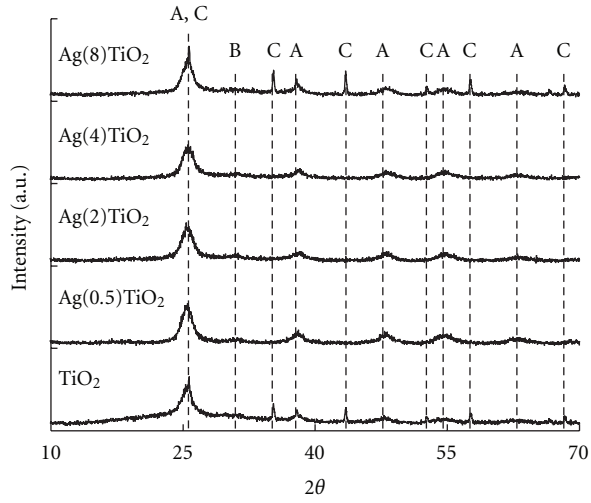

Figure 3: X-ray diffractograms of the TiO_2 and Ag-TiO_2 samples. A: Anatase, B: Brookite, C: Al_2O_3 Corundum.

Table 1: Structural and textural properties of TiO_2 and Ag(2)TiO_2 samples.

Sample	d_{XRD} (Å)	S_{BET} (m^2/g)	d_p (Å)
TiO_2	4.42	370	22.9
Ag(2)TiO_2	3.18	234	19.7

d_{XRD}: calculated crystallite size, S_{BET}: specific surface area, d_p: average pore size.

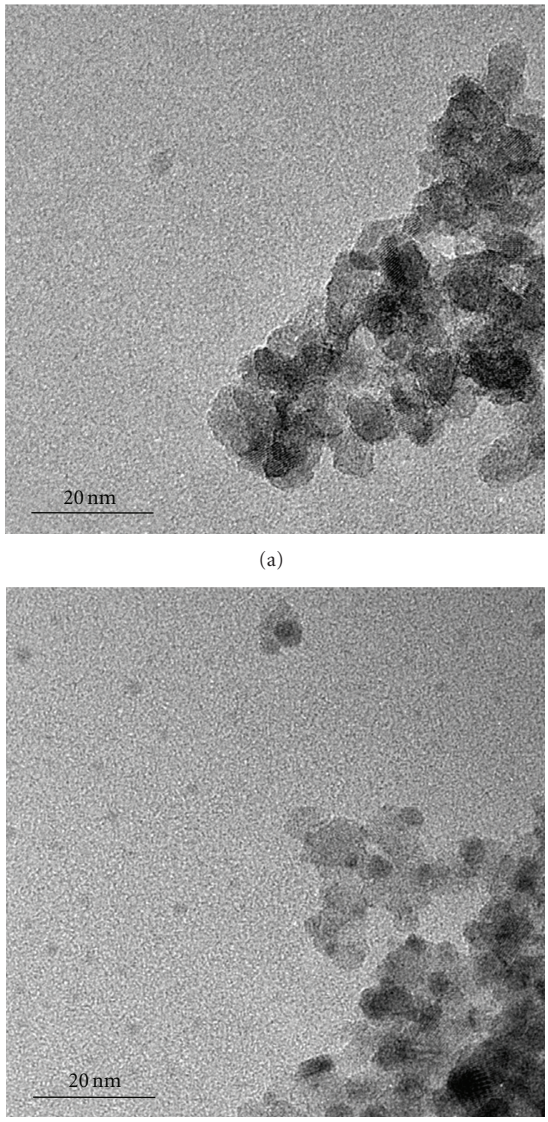

Figure 4: TEM micrographs of the (a) TiO_2 and (b) $Ag(4)TiO_2$ samples. Index (b) is missed in the current phrase.

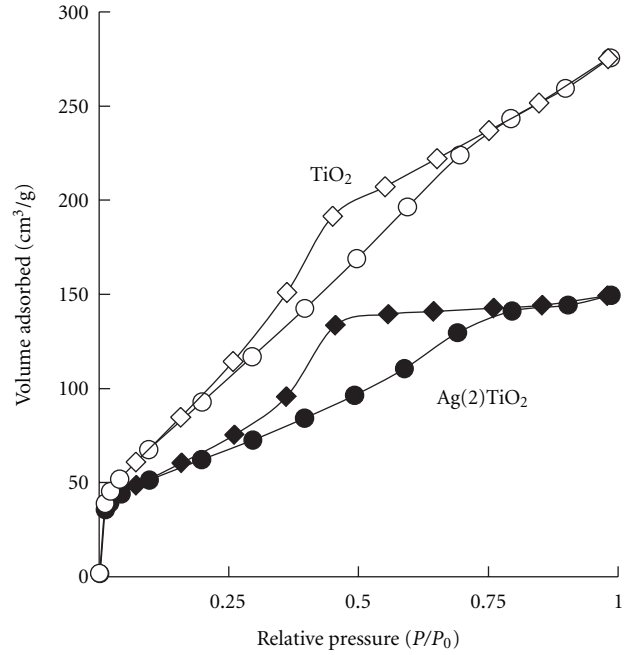

Figure 5: N_2 (●, ○) absorption, (◊, ♦) desorption isotherms of the TiO_2 and $Ag(2)TiO_2$ samples.

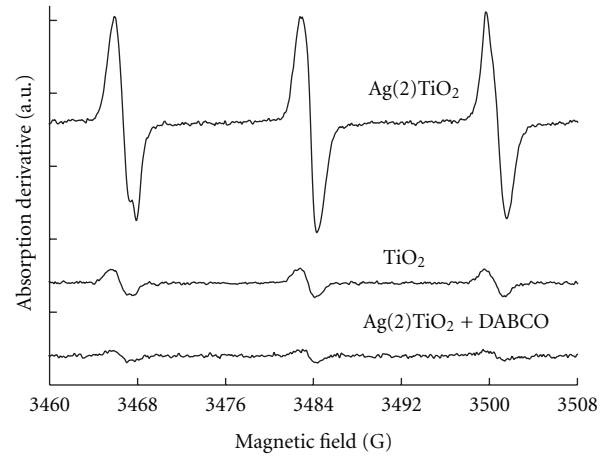

Figure 6: EPR spectra of D_2O suspensions of $Ag(2)TiO_2$ and TiO_2 with TMP-OH and DABCO after 80 min of visible light irradiation.

Figure 6 shows the Ti 2p and Ag 3d XPS spectra of the fresh and solar-simulated light irradiated $Ag(2)TiO_2$ sample. The Ti 2p doublet of the fresh Ag-loaded sample is constituted by Ti $2p_{3/2}$ and Ti $2p_{1/2}$ peaks at 458.9 and 464.6 eV, respectively, indicating a predominant state of Ti^{4+} [41]. Moreover, the Ag 3d spectra of the fresh sample show Ag $3d_{5/2}$ and Ag $3d_{3/2}$ peaks at 368.4 and 374.4 eV, respectively. After peak deconvolution it is observed the presence of two different peaks for $Ag3d_{5/2}$: one at 368.4 eV assigned to Ag^+ [12, 42], while the peak at 368.7 eV is attributed to Ag^0 [12, 43]. Thus, results suggest the coexistence of Ag_2O and Ag^0 probably due to the oxidative action of isopropanol on Ag^+ ions [44] during the synthesis process. Therefore, it is possible to suggest that Ag is deposited on the TiO_2 surface as partially oxidized metallic aggregates. On the other side, the irradiated sample's XPS spectra evidences that the irradiation process shifts signals by ~1.1 eV for the Ag 3d spectra, while that of Ti 2p is shifted by ~1 eV. Ag peaks at 367.2 and 373.2 for Ag $3d_{5/2}$ and Ag $3d_{3/2}$ are assigned to Ag^{2+} species as suggested by Kaushik [45]. In addition, the Ti 2p shift indicates the formation of Ti^{3+} species on the TiO_2 surface [46]. It has been observed that during irradiation of Ag-TiO_2 samples Ag is oxidized by action of photogenerated holes on the TiO_2 VB [47], therefore it is possible to suggest that Ti^{4+} cations, in TiO_2, are reduced by released electrons during Ag oxidation.

Moreover, Ti^{3+} is expected to be rapidly oxidized to Ti^{4+} by surrounding oxygen [48]. However, in this case the chosen synthesis route leads to formation of anatase-brookite mixed

phase oxide with ~50% of amorphous, as early discussed, including organic residues as we have observed in a previous work [4]. Such residues may protect surface oxidation of Ti^{3+} to Ti^{4+} thus allowing its detection in XPS analyses.

3.2. Photocatalytic Production of ROS under Vis Irradiation. Vis-irradiation-induced singlet oxygen ($^1O_2$) formation was monitored by EPR. Figure 7 shows the signal obtained after 50 min of vis irradiation of TiO_2 and Ag(2)TiO_2 suspensions in presence of TMP-OH and DABCO. $^1O_2$ formation was clearly evidenced for Ag(2)TiO_2 with a characteristic 1 : 1 : 1 triplet signal of TEMPOL [49] as depicted in Figure 7. Moreover, the Ag-modified sample revealed an increase in TEMPOL signal thus evidencing a higher $^1O_2$ photoproduction in comparison to TiO_2. Furthermore, the acquired signal of experiments in presence of DABCO revealed a total decrease in the intensity of TEMPOL signal. Since DABCO is a well-known $^1O_2$ scavenger [50] it is possible to confirm its photocatalytic production by action of vis irradiation on Ag(2)TiO_2 suspensions. Therefore, singlet oxygen is promoted by vis-excited Ag aggregates on the TiO_2's surface, and thus it is possible to expect an increased photobactericidal activity of TiO_2.

3.3. Photocatalytic Disinfection of Water and Postirradiation Events. Figure 8(a) shows the bactericidal activity of TiO_2 and Ag-TiO_2 samples in darkness. Results evidence zero toxicity of TiO_2 while Ag(2)TiO_2 and Ag(4)TiO_2 samples totally decreased the *E. coli* population within 180 and 60 min of contact, respectively. Ag ionic species loaded on a substrate's surface have been observed to efficiently inactivate *E. coli* [41]. As a consequence, in our case Ag^+ species are responsible of the bactericidal activity of the Ag-TiO_2 samples under darkness. Moreover, Figure 8(b) shows the evolution of E. coli added to a filtered solution of a 10 h dark-stirred Ag(2)TiO_2 suspension. After 240 min of stirring the filtered solution and *E. coli*, it is observed that bacteria population is affected by the aqueous media. This suggests that Ag^+ ions have been released from the photocatalyst's surface during the dark-stirring process, and after filtration may induce toxicity leading to bacteria death. Then, since the homogeneous bactericidal activity is observed after long times of lixiviation during stirring and the heterogeneous toxicity is observed after 180 min (Figure 8(a)), it seems probable that in-dark contact of the photocatalyst with *E. coli* the bactericidal activity is promoted by the toxicity of Ag+ ions on the photocatalyst surface, and of course, with time released ions play their bactericide role as observed in Figure 8(b). However, an additional heterogeneous photocatalytic effect has been observed to boost inactivation rates under different irradiation setups as discussed earlier.

On the other side, Figure 9 shows the photodisinfection tests results under 250 and 750 W/m^2 of solar-simulated light irradiation of Ag-TiO_2 samples and their correspondent EDT_{24}. Figures 9(a) and 9(b) show the performance of TiO_2- and Ag-modified samples: Ag(2)TiO_2 and Ag(4)TiO_2. The increase in Ag loading effectively enhanced the photodisinfecting effect of TiO_2. Moreover, the *E. coli* inactivation rates are boosted when increasing the irradiation power thus confirming the heterogeneity of the photocatalytic process as observed in Figure 9(b). Indeed, under 250 W/m^2 the Ag(2)TiO_2 sample reaches total inactivation within 20 min,

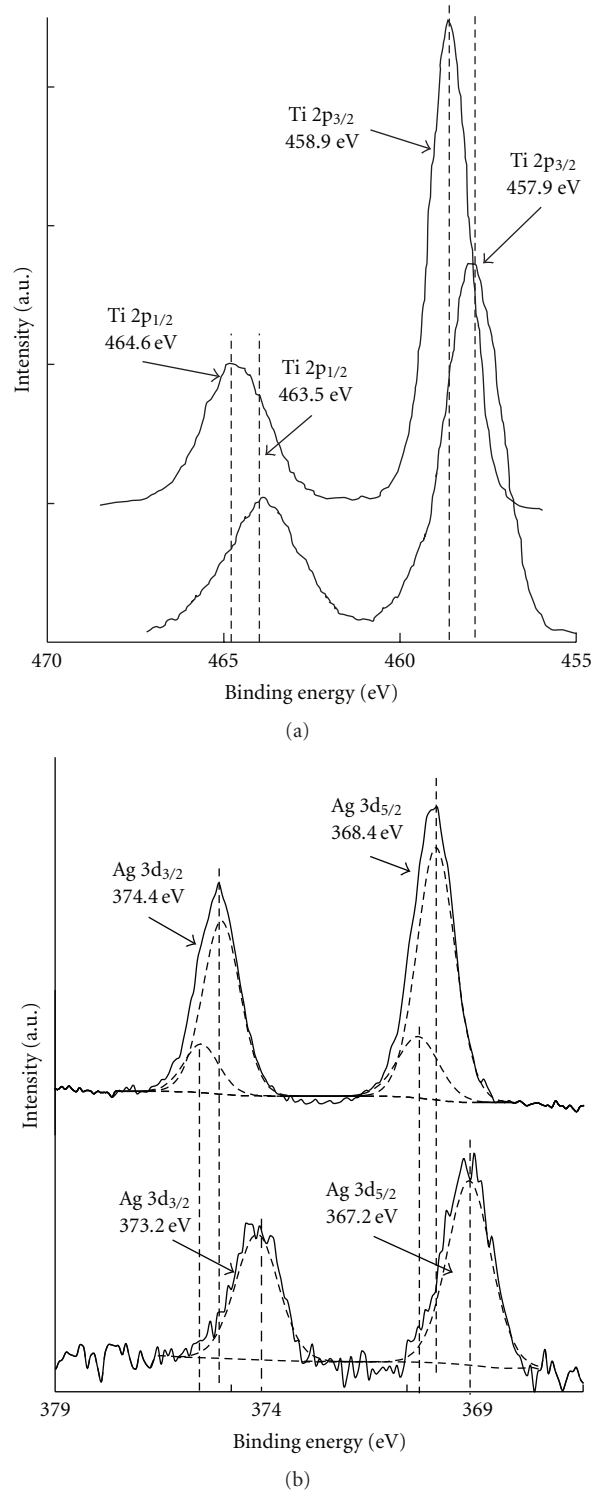

Figure 7: XPS spectra of (a) the Ti 2p region of the TiO_2 and Ag(2)TiO_2 samples and (b) the Ag 3d region of the Ag(2)TiO_2 (top) and solar-simulated light irradiated Ag(2)TiO_2 (bottom) samples.

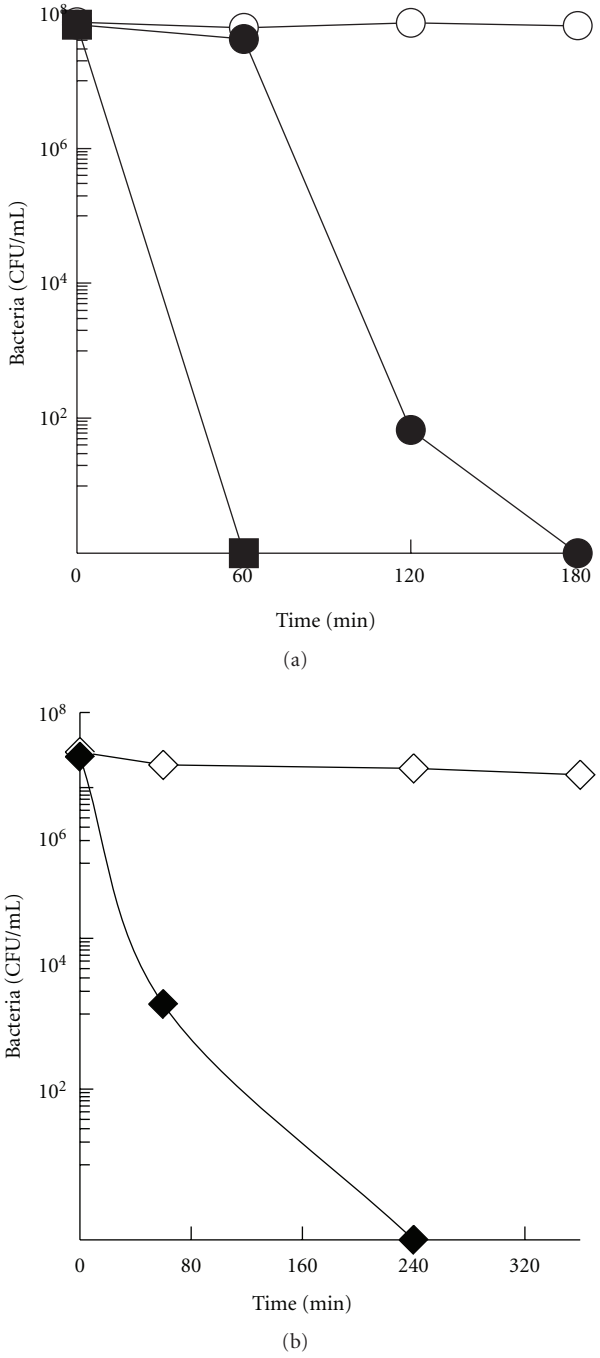

Figure 8: Dark events of *E. coli* with (a) (■) $Ag(4)TiO_2$, (●) $Ag(2)TiO_2$, and (◯) TiO_2 samples and (b) filtered solutions of previously 10 h stirred suspensions of (◆) $Ag(2)TiO_2$, and (◇) TiO_2.

while the bactericidal effect reduced the population in 60 min (Figure 8). This effect is observed to increase under 400 W/m^2 of irradiation since the total inactivation, by the same sample, is reached after 10 min. Then, the photocatalytic effect decreases the inactivation time by 40 and 50 min, under 250 and 400 W/m^2, respectively, indicating that the total bactericidal action is a sum of photoinduced processes and photocatalysts toxicity.

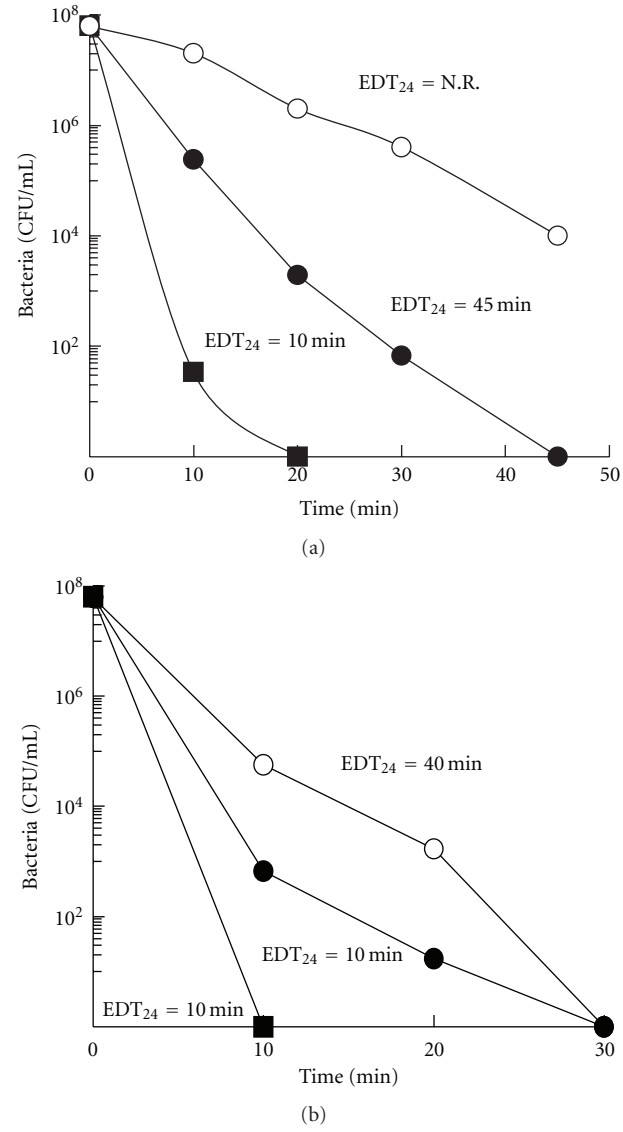

Figure 9: Photocatalytic water disinfection using: (■) $Ag(4)TiO_2$, (●) $Ag(2)TiO_2$ and (◯) TiO_2 samples, under (a) 250 and (b) 400 W/m^2 of solar-simulated light irradiation.

Furthermore, using irradiation of interior lighting lamps similar effects were observed. Such photocatalytic process can now be correlated to the photoproduction of ROS. As it was previously observed, the spectrum of the Xenon lamp has a ~50% of irradiance power correspondent to visible light, and even more, the excitation wavelength of the Ag nanoparticles on the TiO_2 surface is emitted by this source (~470 nm), thus singlet oxygen is produced. A vast majority of cell types, from prokaryotic to mammalian, undergo irreversible damage leading to cell death by exposure to singlet oxygen [51, 52], therefore in our case the *E. coli* inactivation is attributed to $^1O_2$ photoproduction.

Moreover, samples of these experiments were kept in dark during 24 h and bacteria concentration was measured to determine the EDT_{24}. It is observed that 10 min of solar-simulated light irradiation are required to achieve inactivation

without regrowth using the Ag(4)TiO_2 sample, even if 10 min of irradiation do not lead to total inactivation as observed in Figure 9(a). On the other hand, the performance of Ag(2)TiO_2 leads to an EDT_{24} of 45 min while that of TiO_2 was not reached during the irradiation time. A similar effect was observed with 400 W/m^2 of irradiation as observed in Figure 9(b). However, in this case using TiO_2 and Ag(2)TiO_2 samples the correspondent EDT_{24} were 10 and 40 min, respectively, suggesting an increase in the effective oxidative action of the photocatalysts when increasing the irradiation power [53].

Furthermore, Figure 10 shows the results of the photocatalytic water disinfection using the TiO_2 and $AgTiO_2$ samples under irradiation of 9.8 W/m^2 of natural sunshine irradiation from interior-lighting lamps. Results evidence a fast decay of the *E. coli* concentration using the Ag(4)TiO_2 sample, while Ag(2)TiO_2 and TiO_2 show lower performances. Such behavior was expected since the light irradiation setup, as previously discussed, has a wide peak of light irradiation at 470 nm which may effectively activate the photocatalyst surface as presented in Figure 2. Nevertheless, the EDT_{24} were diminished of course due to the decrease in light irradiation power.

It has been previously discussed that during the photocatalytic inactivation of *E. coli* it is necessary to achieve a sum of damages to achieve the complete inactivation of bacteria [54]. Moreover, Rincón and Pulgarin [53] have discussed that even achieving total inactivation during irradiation it is possible to observe regrowth of the bacteria population, after 24 h in dark, indicating that somehow the level of damage needed for absolute death has not been reached. Therefore, in our case we have observed that using Ag modified particles it is possible to achieve a true inactivation in short irradiation periods, as observed after dark periods of 24 h, even without reaching zero concentration of bacteria during irradiation. Such effect, as earlier discussed, is due to action of photoinduced and bactericidal processes.

Finally, to discuss photocatalyst stability it is possible to expect that loosing active silver species on the photocatalyst's surface, during stirring, may lead to a less active surface photocatalysts, and therefore, studies focusing on improving Ag fixing and stability on TiO_2 should be developed.

4. Conclusions

Ag-TiO_2 photocatalysts, synthesized using the hydrothermal synthesis, lead to Ag aggregates on the TiO_2 surface which increases the visible light response of TiO_2. In addition, such aggregates are partially oxidized particles that distorted the pore distribution of the samples. This photocatalyst configuration seems to promote photoactivity towards the photocatalytic disinfection of water under solar light and interior-light irradiations. Photoactivity was effectively correlated to the photoproduction of singlet oxygen under visible light irradiation as determined by EPR analyses using DABCO as a singlet oxygen quencher. Moreover, analysis of dark processes evidenced that part of the inactivation process is due to the bactericidal effect of silver in the surface and possible lixiviated Ag^+ ions.

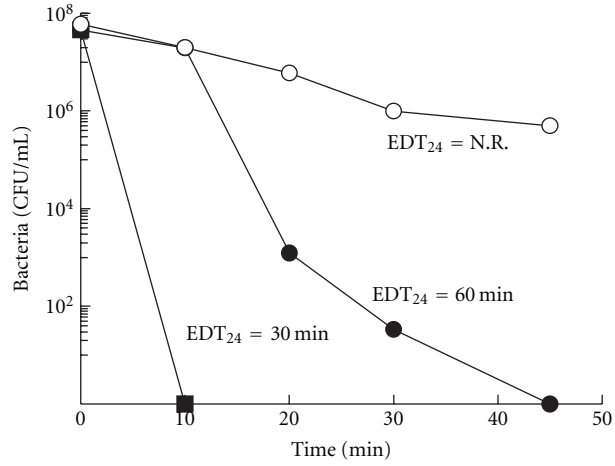

Figure 10: Photocatalytic water disinfection using (■) Ag(4)TiO_2, (●) Ag(2)TiO_2, and (◯) TiO_2 samples, under 9.8 W/m^2 of natural sunshine light irradiation of interior lighting.

Acknowledgments

The authors express their gratitude to Professor Aristóbulo Centeno, R.I.P, for his valuable life and academic advice. They still spread the research spirit he sowed on them. This work was financially supported by UIS through the project: Fijación de semiconductors sobre poliéster para obtención de textiles fotobactericidas, code: 5448. C. Castro thanks also A. Colciencias, Sena, and UIS for financial support to his finished Ph.D. studies. Special acknowledgments are to the Group of Electrochemical Engineering and the Laboratory of Complex Matter Physics, in the EPFL, Switzerland, for the XPS and EPR analyses.

References

[1] J. A. Byrne, P. A. Fernandez-Ibañez, P. S.M. Dunlop, D. M.A. Alrousan, and J. W.J. Hamilton, "Photocatalytic enhancement for solar disinfection of water: a review," *International Journal of Photoenergy*, vol. 2011, Article ID 798051, 12 pages, 2011.

[2] S.-J. Kim, N.-H. Lee, H.-J. Oh, S.-C. Jung, W.-J. Lee, and D.-H. Kim, "Photocatalytic properties of nanotubular-shaped TiO_2 powders with anatase phase obtained from titanate nanotube powder through various thermal treatments," *International Journal of Photoenergy*, vol. 2011, Article ID 327821, 7 pages, 2011.

[3] C. Wang and J. Yao, "Decolorization of methylene blue with TiO_2 sol via UV irradiation photocatalytic degradation," *International Journal of Photoenergy*, vol. 2010, Article ID 643182, 6 pages, 2010.

[4] C. A. Castro, A. Centeno, and S. A. Giraldo, "Iron promotion of the TiO_2 photosensitization process towards the photocatalytic oxidation of azo dyes under solar-simulated light irradiation," *Materials Chemistry and Physics*, vol. 129, no. 3, pp. 1176–1183, 2011.

[5] A. J. Frank, N. Kopidakis, and J. V. D. Lagemaat, "Electrons in nanostructured TiO_2 solar cells: transport, recombination and photovoltaic properties," *Coordination Chemistry Reviews*, vol. 248, no. 13-14, pp. 1165–1179, 2004.

[6] C. A. Castro-López, A. Centeno, and S. A. Giraldo, "Fe-modified TiO_2 photocatalysts for the oxidative degradation of recalcitrant water contaminants," *Catalysis Today*, vol. 157, no. 1-4, pp. 119–124, 2010.

[7] J. Gamage and Z. Zhang, "Applications of photocatalytic disinfection," *International Journal of Photoenergy*, vol. 2010, Article ID 764870, 11 pages, 2010.

[8] A. G. Rincón, C. Pulgarin, N. Adler, and P. Peringer, "Interaction between *E. coli* inactivation and DBP-precursors-dihydroxybenzene isomers in the photocatalytic process of drinking-water disinfection with TiO_2," *Journal of Photochemistry and Photobiology A*, vol. 139, no. 2-3, pp. 233–241, 2001.

[9] M. K. Seery, R. George, P. Floris, and S. C. Pillai, "Silver doped titanium dioxide nanomaterials for enhanced visible light photocatalysis," *Journal of Photochemistry and Photobiology A*, vol. 189, no. 2-3, pp. 258–263, 2007.

[10] K. Awazu, M. Fujimaki, C. Rockstuhl et al., "A plasmonic photocatalyst consisting of silver nanoparticles embedded in titanium dioxide," *Journal of the American Chemical Society*, vol. 130, no. 5, pp. 1676–1680, 2008.

[11] B. Xin, L. Jing, Z. Ren, B. Wang, and H. Fu, "Effects of simultaneously doped and deposited Ag on the photocatalytic activity and surface states of TiO_2," *Journal of Physical Chemistry B*, vol. 109, no. 7, pp. 2805–2809, 2005.

[12] O. Akhavan and E. Ghaderi, "Self-accumulated Ag nanoparticles on mesoporous TiO_2 thin film with high bactericidal activities," *Surface and Coatings Technology*, vol. 204, no. 21-22, pp. 3676–3683, 2010.

[13] Z. Xiong, J. Ma, W. J. Ng, T. D. Waite, and X. S. Zhao, "Silver-modified mesoporous TiO_2 photocatalyst for water purification," *Water Research*, vol. 45, no. 5, pp. 2095–2103, 2011.

[14] W. Zhou, H. Liu, J. Wang, D. Liu, G. Du, and J. Cui, "Ag2O/TiO_2 nanobelts heterostructure with enhanced ultraviolet and visible photocatalytic activity," *ACS Applied Materials & Interfaces*, vol. 2, no. 8, pp. 2385–2392, 2010.

[15] D. R. Monteiro, L. F. Gorup, A. S. Takamiya, A. C. Ruvollo-Filho, E. R. D. Camargo, and D. B. Barbosa, "The growing importance of materials that prevent microbial adhesion: antimicrobial effect of medical devices containing silver," *International Journal of Antimicrobial Agents*, vol. 34, no. 2, pp. 103–110, 2009.

[16] Y. Lai, Y. Chen, H. Zhuang, and C. Lin, "A facile method for synthesis of Ag/TiO_2 nanostructures," *Materials Letters*, vol. 62, no. 21-22, pp. 3688–3690, 2008.

[17] L. Miao, Y. Ina, S. Tanemura et al., "Fabrication and photochromic study of titanate nanotubes loaded with silver nanoparticles," *Surface Science*, vol. 601, no. 13, pp. 2792–2799, 2007.

[18] A. Zielińska, E. Kowalska, J. W. Sobczak et al., "Silver-doped TiO_2 prepared by microemulsion method: surface properties, bio- and photoactivity," *Separation and Purification Technology*, vol. 72, no. 3, pp. 309–318, 2010.

[19] Y. Liu, C. Y. Liu, Q. H. Rong, and Z. Zhang, "Characteristics of the silver-doped TiO_2 nanoparticles," *Applied Surface Science*, vol. 220, no. 1–4, pp. 7–11, 2003.

[20] J. Yu, J. Xiong, B. Cheng, and S. Liu, "Fabrication and characterization of Ag-TiO_2 multiphase nanocomposite thin films with enhanced photocatalytic activity," *Applied Catalysis B*, vol. 60, no. 3-4, pp. 211–221, 2005.

[21] G. Oliveri, G. Ramis, G. Busca, and V. S. Escribano, "Thermal stability of vanadia-titania catalysts," *Journal of Materials Chemistry*, vol. 3, no. 12, pp. 1239–1249, 1993.

[22] M. Kusakabe, Y. Ito, M. Arai, Y. Shirakawa, and S. Tamaki, "Ionic conductivity in silver-dissolved α-CuI," *Solid State Ionics*, vol. 92, no. 1-2, pp. 135–138, 1996.

[23] J. Maier, *Physical Chemistry of Ionic Materials: Ions and Electrons in Solids*, Wiley, London, UK, 2004.

[24] M. C. Biesinger, L. W. M. Lau, A. R. Gerson, and R. S. C. Smart, "Resolving surface chemical states in XPS analysis of first row transition metals, oxides and hydroxides: Sc, Ti, V, Cu and Zn," *Applied Surface Science*, vol. 257, no. 3, pp. 887–898, 2010.

[25] M. Stylidi, D. I. Kondarides, and X. E. Verykios, "Visible light-induced photocatalytic degradation of Acid Orange 7 in aqueous TiO_2 suspensions," *Applied Catalysis B*, vol. 47, no. 3, pp. 189–201, 2004.

[26] Y. E. Nesmelov and D. D. Thomas, "Multibore sample cell increases EPR sensitivity for aqueous samples," *Journal of Magnetic Resonance*, vol. 178, no. 2, pp. 318–324, 2006.

[27] Q. Chang, H. He, and Z. Ma, "Efficient disinfection of *Escherichia coli* in water by silver loaded alumina," *Journal of Inorganic Biochemistry*, vol. 102, no. 9, pp. 1736–1742, 2008.

[28] H. Gerischer and A. Heller, "The role of oxygen in photooxidation of organic molecules on semiconductor particles," *Journal of Physical Chemistry*, vol. 95, no. 13, pp. 5261–5267, 1991.

[29] Y. Tian and T. Tatsuma, "Plasmon-induced photoelectrochemistry at metal nanoparticles supported on nanoporous TiO_2," *Chemical Communications*, vol. 10, no. 16, pp. 1810–1811, 2004.

[30] M. Richter, A. Abramova, U. Bentrup, and R. Fricke, "Proof of reversible Ag^+/Ag^0 redox transformation on mesoporous alumina by in situ UV-Vis spectroscopy," *Journal of Applied Spectroscopy*, vol. 71, no. 3, pp. 400–403, 2004.

[31] G. A. Ozin, F. Hugues, S. M. Mattar, and D. F. McIntos, "Low nuclearity silver clusters in fajausite-type zeolites: optical spectroscopy, photochemistry, and relationship to the photodimerization of alkanes," *Journal of Physical Chemistry*, vol. 87, no. 18, pp. 3445–3450, 1983.

[32] B. Cheng, Y. Le, and J. Yu, "Preparation and enhanced photocatalytic activity of Ag@TiO_2 core-shell nanocomposite nanowires," *Journal of Hazardous Materials*, vol. 177, no. 1–3, pp. 971–977, 2010.

[33] Q. Xiang, J. Yu, B. Cheng, and H. C. Ong, "Microwave-hydrothermal preparation and visible-light photoactivity of plasmonic photocatalyst Ag-TiO_2 nanocomposite hollow spheres," *Chemistry—An Asian Journal*, vol. 5, no. 6, pp. 1466–1474, 2010.

[34] Z. Zheng, B. Huang, X. Qin, X. Zhang, Y. Dai, and M. -H. Whangbo, "Facile in situ synthesis of visible-light plasmonic photocatalysts M@TiO_2 (M = Au, Pt, Ag) and evaluation of their photocatalytic oxidation of benzene to phenol," *Journal of Materials Chemistry*, vol. 21, no. 25, pp. 9079–9087, 2011.

[35] P. Wang, B. Huang, X. Qin et al., "Ag@AgCl: a highly efficient and stable photocatalyst active under visible light," *Angewandte Chemie*, vol. 47, no. 41, pp. 7931–7933, 2008.

[36] B. Baruwati and R. S. Varma, "Synthesis of N-doped nano TiO_2 using guanidine nitrate: an excellent visible light photocatalyst," *Journal of Nanoscience and Nanotechnology*, vol. 11, no. 3, pp. 2036–2041, 2011.

[37] R. Jin, Y. Cao, C. A. Mirkin, K. L. Kelly, G. C. Schatz, and J. G. Zheng, "Photoinduced conversion of silver nanospheres to nanoprisms," *Science*, vol. 294, no. 5548, pp. 1901–1903, 2001.

[38] X. Wang, S. Li, H. Yu, and J. Yu, "In situ anion-exchange synthesis and photocatalytic activity of Ag 8W4O16/AgCl-nanoparticle core-shell nanorods," *Journal of Molecular Catalysis A*, vol. 334, no. 1-2, pp. 52–59, 2011.

[39] W. Zhao, L. Feng, R. Yang, J. Zheng, and X. Li, "Synthesis, characterization, and photocatalytic properties of Ag modified hollow SiO_2/TiO_2 hybrid microspheres," *Applied Catalysis B*, vol. 103, no. 1-2, pp. 181–189, 2011.

[40] F. B. Li, X. Z. Li, C. H. Ao, S. C. Lee, and M. F. Hou, "Enhanced photocatalytic degradation of VOCs using $Ln3^{+}$-TiO_2 catalysts for indoor air purification," *Chemosphere*, vol. 59, no. 6, pp. 787–800, 2005.

[41] O. Akhavan, "Lasting antibacterial activities of Ag-TiO_2/Ag/a-TiO_2 nanocomposite thin film photocatalysts under solar light irradiation," *Journal of Colloid and Interface Science*, vol. 336, no. 1, pp. 117–124, 2009.

[42] M. Romand, M. Roubin, and J. P. Deloume, "ESCA studies of some copper and silver selenides," *Journal of Electron Spectroscopy and Related Phenomena*, vol. 13, no. 3, pp. 229–242, 1978.

[43] B. Xin, Z. Ren, H. Hu et al., "Photocatalytic activity and interfacial carrier transfer of Ag-TiO_2 nanoparticle films," *Applied Surface Science*, vol. 252, no. 5, pp. 2050–2055, 2005.

[44] Z. Y. Huang, G. Mills, and B. Hajek, "Spontaneous formation of silver particles in basic 2-propanol," *Journal of Physical Chemistry*, vol. 97, no. 44, pp. 11542–11550, 1993.

[45] V. K. Kaushik, "XPS core level spectra and Auger parameters for some silver compounds," *Journal of Electron Spectroscopy and Related Phenomena*, vol. 56, no. 3, pp. 273–277, 1991.

[46] F. Werfel and O. Brümmer, "Corundum structure oxides studied by XPS," *Physica Scripta*, vol. 28, no. 1, pp. 92–96, 1983.

[47] A. Romanyuk and P. Oelhafen, "Formation and electronic structure of TiO_2-Ag interface," *Solar Energy Materials and Solar Cells*, vol. 91, no. 12, pp. 1051–1054, 2007.

[48] N. Sakai, R. Wang, A. Fujishima, T. Watanabe, and K. Hashimoto, "Effect of ultrasonic treatment on highly hydrophilic TiO_2 surfaces," *Langmuir*, vol. 14, no. 20, pp. 5918–5920, 1998.

[49] R. Konaka, E. Kasahara, W. C. Dunlap, Y. Yamamoto, K. C. Chien, and M. Inoue, "Irradiation of titanium dioxide generates both singlet oxygen and superoxide anion," *Free Radical Biology and Medicine*, vol. 27, no. 3-4, pp. 294–300, 1999.

[50] S. Kaur and V. Singh, "Visible light induced sonophotocatalytic degradation of Reactive Red dye 198 using dye sensitized TiO_2," *Ultrasonics Sonochemistry*, vol. 14, no. 5, pp. 531–537, 2007.

[51] T. A. Dahl, "Direct exposure of mammalian cells to pure exogenous singlet oxygen ($\Delta_g O_2$)," *Photochemistry and Photobiology*, vol. 57, no. 2, pp. 248–254, 1993.

[52] Z. Cheng and Y. Li, "What is responsible for the initiating chemistry of iron-mediated lipid peroxidation: an update," *Chemical Reviews*, vol. 107, no. 3, pp. 748–766, 2007.

[53] A. G. Rincón and C. Pulgarin, "Bactericidal action of illuminated TiO_2 on pure Escherichia coli and natural bacterial consortia: post-irradiation events in the dark and assessment of the effective disinfection time," *Applied Catalysis B*, vol. 49, no. 2, pp. 99–112, 2004.

[54] J. Marugán, R. van Grieken, C. Sordo, and C. Cruz, "Kinetics of the photocatalytic disinfection of Escherichia coli suspensions," *Applied Catalysis B*, vol. 82, no. 1-2, pp. 27–36, 2008.